*Inorg. Chem.* **2007**, *46*, 3826–3838


# A Density Functional Theory Study of the Reaction of the Biomimetic Iron(II) Complex of a Tetradentate Bispidine Ligand with $H_2O_2$

**Peter Comba,* Gopalan Rajaraman, and Heidi Rohwer**

*Universität Heidelberg, Anorganisch-Chemisches Institut, Im Neuenheimer Feld 270, D-69120 Heidelberg, Germany*

Received June 22, 2006

Three pathways for the reaction of bispidine-iron(II) complexes (where bispidine is a rigid tetradentate amine/pyridine ligand) with $H_2O_2$ have been studied by DFT calculations. For all oxidation states the high-spin and low-spin (intermediate-spin) forms have been optimized, and the computed data have been compared with the readily available experimental results. It is concluded that there is a direct conversion of the bispidine-iron(II)-hydrogen peroxide complex to the corresponding iron(IV)-dihydroxo compound, which is a novel possible oxidant for the dihydroxylation of olefins.

## Introduction

Mononuclear non-heme iron enzymes are known to catalyze a variety of hydrocarbon oxidations by the activation of molecular oxygen,[1−3] and much research has been devoted to clarify the mechanisms of these reactions. While detailed mechanisms remain unclear in many cases, end-on $Fe^{III}$-alkylperoxo or -hydroperoxo and $Fe^{IV}$-oxo complexes have been characterized and are believed to be important intermediates. However, for mononuclear non-heme iron biomolecules, few reactive intermediates have been fully characterized. Key intermediates that have been identified include a high-spin $Fe^{III}$-alkylperoxo unit in lipoxygenase,[2,4,5] a low-spin $Fe^{III}$-hydroperoxo intermediate in bleomycin,[6,7] and a high-spin $Fe^{IV}$═O species in TauD (an α-ketoglutarate dioxygenase enzyme).[8] While heterolytic cleavage of the O−O bond of the $Fe^{III}OOH$ intermediate has been shown by DFT calculations to be highly favorable for porphyrin systems,[2,9,10] due to the formation of an $Fe^{IV}$═O/porphyrin radical combination, O−O bond heterolysis in the non-heme iron enzyme and antitumor drug bleomycin is calculated to be highly endothermic and therefore unlikely to play a role. Homolytic cleavage has also been ruled out with bleomycin on the basis of the high specificity of the reaction of bleomycin with DNA.[7] The belief therefore was that the $Fe^{III}$-hydroperoxo intermediate in bleomycin is directly responsible for attack on the substrate. In a very recent DFT-based study, alternative mechanisms which involve high valent oxo-iron complexes are proposed.[11]

In addition to the biological studies, the development of synthetic iron complexes, aimed at mimicking the oxygenation reactions observed in non-heme iron oxygenases and at the development of efficient oxidation catalysts, is an active area of research.[3,12] In particular, a number of tetra- and pentadentate ligands with amine/pyridine donor sets have been synthesized, whose iron(II) complexes have shown activity in the oxidation of alkanes and olefins in the presence of hydrogen peroxide. The $Fe^{II}$ complexes of some bispidine ligands have also been tested in the catalytic epoxidation and dihydroxylation of olefins with $H_2O_2$ and have proven to be among the most active catalysts, comparable in activity to those of tris(2-pyridylmethyl)amine (tpa) and its deriva-

* To whom correspondence should be addressed. E-mail: peter.comba@aci.uni-heidelberg.de. Fax: +49-6221-54-66 17.

(1) Feig, A. L.; Lippard, S. J. *Chem. Rev.* **1994**, *94*, 759.
(2) Solomon, E. I.; Brunold, T. C.; Davis, M. I.; Kensley, J. N.; Lee, S.-K.; Lehnert, N.; Neese, F.; Skulan, A. J.; Yang, Y.-S.; Zhou, J. *Chem. Rev.* **2000**, *100*, 235.
(3) Costas, M.; Mehn, M. P.; Jensen, M. P.; Que, L., Jr. *Chem. Rev.* **2004**, *104*, 939.
(4) Que L., Jr.; Ho, R. Y. N. *Chem. Rev.* **1996**, *96*, 2607.
(5) Skrzypczak-Jankun, E.; Bross, R. A.; Caroll, R. T.; Dunham, W. R.; Funk, M. O., Jr. *J. Am. Chem. Soc.* **2001**, *123*, 10814.
(6) Westre, T. E.; Loeb, K. E.; Zaleski, J. M.; Hedman, B.; Hodgson, K. O.; Solomon, E. I. *J. Am. Chem. Soc.* **1995**, *117*, 1309.
(7) Neese, F.; Zaleski, J. M.; Loeb Zaleski, K.; Solomon, E. I. *J. Am. Chem. Soc.* **2000**, *122*, 11703.
(8) Price, J. C.; Barr, E. W.; Tirupati, B.; Bollinger, M., Jr.; Krebs, C. *Biochemistry* **2003**, *42*, 7497.
(9) Harris, D. L.; Loew, G. H. *J. Am. Chem. Soc.* **1998**, *120*, 8941.
(10) Meunier, B.; de Visser, S. P.; Shaik, S. *Chem. Rev.* **2004**, *104*, 3947.
(11) Kumar, D.; Hirao, H.; Shaik, S.; Kozlowski, P. M. *J. Am. Chem. Soc.* **2006**, *128*, 16148.
(12) Que, L., Jr. *J. Chem. Soc., Dalton Trans.* **1997**, *21*, 3933.



10.1021/ic061129y CCC: $37.00 
Published on Web 04/11/2007

**Chart 1**

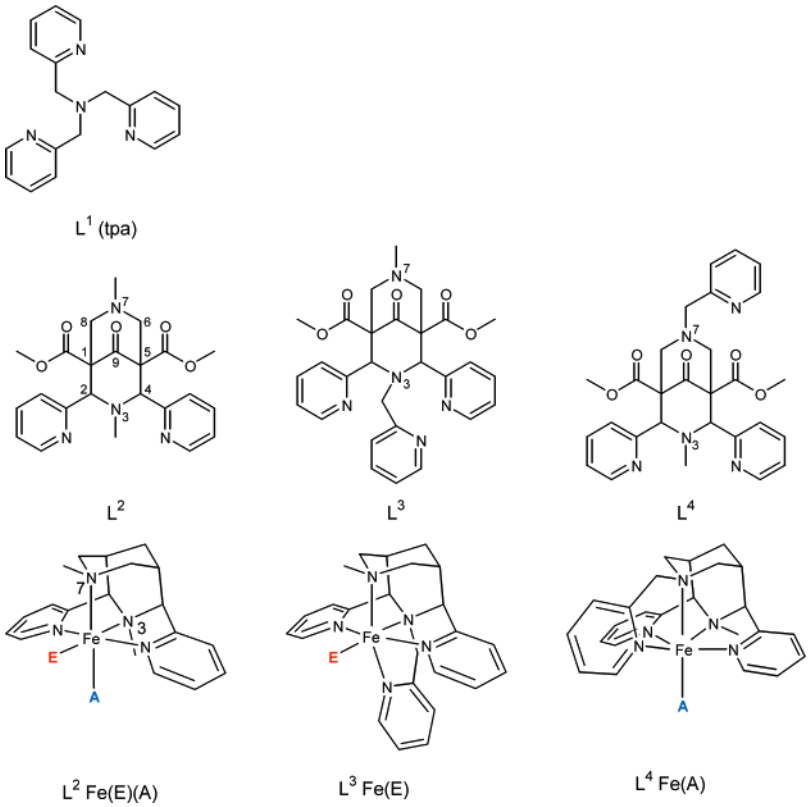


tives (see Chart 1 for ligand structures).[13] They have distorted cis-octahedral geometries, with one or two open coordination sites, which differ in their ability to bind substrates.[14] Coordination in the equatorial plane trans to N3 (E in Chart 1) leads to short and strong bonds, while axial coordination trans to N7 (A in Chart 1) leads to longer and weaker bonds.[15] While in complexes with $L^2$ both coordination sites are available, in complexes with $L^3$ and $L^4$ one of these (trans to N3 and N7, respectively) is blocked, leading to strong differences in reactivity.

On the basis of product distributions, labeling studies, and spectroscopically characterized intermediates, a similar chemistry is assumed for $L^3$ and $L^4$. For both ligands, low-spin $Fe^{III}$-$\eta^1$-hydroperoxo, high-spin $Fe^{III}$-$\eta^2$-peroxo, and intermediate-spin ($S = 1$) $Fe^{IV}$═O intermediates have been characterized spectroscopically in the reaction of their $Fe^{II}$ complexes with $H_2O_2$ under various conditions, and the ferryl complex in particular has been identified as the important oxidant for olefins.[13,15,16] However, no $Fe^{III}$ and $Fe^{IV}$ intermediates have been trapped and characterized so far in the reaction of the $Fe^{II}$ complex of $L^2$ with $H_2O_2$, although $Fe^{III}$-alkylperoxo complexes are formed in the reaction with $^t$BuOOH.[17] There also is a marked difference between the catalysts based on $L^2$ and $L^4$ in terms of the product distributions and labeling results in the catalytic olefin oxidation.[13,18] The most important differences are that (i) a large part of the oxidation products is due to a radical pathway with the catalyst based on $L^4$, and this is much less pronounced for $L^2$, and (ii) with the $L^2$-based catalyst, both $H_2O_2$ oxygen atoms are transferred to the diol products which in contrast to the $L^4$-based catalyst selectively are cis-configured, with close to 100% efficiency. These experimental facts, together with the recent observation that with $L^3$ there is direct oxidation of $Fe^{II}$ to $Fe^{IV}$═O with $H_2O_2$ in aqueous solution,[16] a mechanism which is supported by DFT calculations on the $Fe^{II}$ aqua ion,[19,20] and the fact that no high valent iron species are observed in $Fe^{II}L^2/H_2O_2$ reactions, initiated the present DFT study. Our aim here is to identify the most favorable pathways and the corresponding products of the $Fe^{II}L^2/H_2O_2$ oxidation in the absence of olefin substrates.

Scheme 1 shows the three mechanistic pathways that have been investigated for the $L^2$-based $Fe^{II}$ system. Pathway A is based on the formation of an $Fe^{III}$ intermediate, while pathways B and C are based on the direct transformation of $Fe^{II}$ to $Fe^{IV}$ complexes. The results are compared with available experimental information. Possible reasons for the differences in behavior between $L^2$ and other tetradentate

(13) Bukowski, M. R.; Comba, P.; Lienke, A.; Limberg, C.; Lopez de Laorden, C.; Mas-Balleste, R.; Merz, M.; Que, L., Jr. *Angew. Chem., Int. Ed.* **2006**, *45*, 3446.
(14) Börzel, H.; Comba, P.; Hagen, K. S.; Merz, M.; Lampeka, Y. D.; Lienke, A.; Linti, G.; Pritzkow, H.; Tsymbal, L. V. *Inorg. Chim. Acta* **2002**, *337*, 407.
(15) Bukowski, M. R.; Comba, P.; Limberg, C.; Merz, M.; Que, L., Jr.; Wistuba, T. *Angew. Chem., Int. Ed.* **2004**, *43*, 1283.
(16) Bautz, J.; Bukowski, M.; Kerscher, M.; Stubna, A.; Comba, P.; Lienke, A.; Münck, E.; Que, L., Jr. *Angew. Chem., Int. Ed.* **2006**, *45*, 5681.
(17) Bautz, J.; Comba, P.; Que, L., Jr. *Inorg. Chem.* **2006**, *45*, 7077.
(18) Bautz, J.; Comba, P.; Lopez de Laorden, C.; Menzel, M.; Rajaraman, G. To be submitted for publication.
(19) Buda, F.; Ensing, B.; Baerends, E. *J. Phys. Chem. A* **2003**, *107*, 5722.
(20) Buda, F.; Ensing, B.; Gribnau, M. C. M.; Baerends, E. J. *Chem.—Eur. J.* **2003**, *9*, 3436.

**Scheme 1**

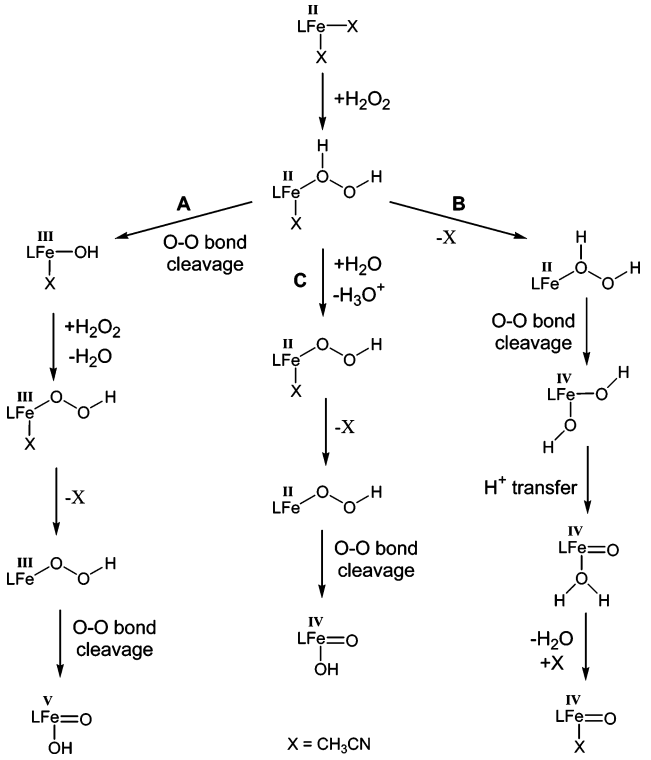


ligands such as $L^1$, as well as the pentadentate bispidine ligands $L^3$ and $L^4$, are also discussed.

## Computational Methods

Calculations were performed with Gaussian 03[21] using DFT methods. Geometries were optimized in the gas phase using the B3LYP functional[22,23] and a 6-31G(d) basis set. Frequency calculations were performed on the optimized structures to verify that they are minima on the PES and also to obtain zero-point energy corrections. Selected structures were reoptimized with the same functional and basis set but including solvent effects via the polarized continuum model (PCM)[24−27] with acetonitrile as the solvent. The difference in geometry between the gas phase and the solvated structures was less than 0.02 Å for the bond lengths and less than 4° for the angles, and solvent effects were therefore neglected for further geometry optimizations. Single point energy calculations were performed on the B3LYP/6-31G(d) optimized structures using Ahlrich's TZVPP basis set[28] and including solvent effects as described above. The quoted energies are those calculated at the B3LYP/TZVPP level, with zero-point and free energy corrections (enthalpy and entropy) from the frequency calculations at the B3LYP/6-31G(d) level.[29] A simplified model system was used in all calculations, in which the ester groups at C1 and C5 on the ligand backbone were replaced by hydrogen atoms.

The ligand $L^2$ is tetradentate, and the corresponding complex therefore has two possible substrate coordination sites. Coordination of the substrate is assumed to take place trans to the tertiary amine N3 (E in Chart 1), as this has been shown to be the favored coordination site in complexes of $L^2$. This assumption has nonetheless been tested and confirmed for selected complexes by calculating the relative energies of the two possible isomers (trans to N3 and trans to N7). The oxidation reactions and catalytic oxidations are generally performed in MeOH, $CH_3CN$, or $H_2O$, using a $Fe^{II}-H_2O_2$-(−cyclooctene substrate) ratio of 1:10(:1000). Since an aqueous solution of $H_2O_2$ is used, small amounts of $H_2O$ are found in all solutions. Only solvation in $CH_3CN$ is considered here, but the possibility of coordination of $CH_3CN$ or $H_2O$ in the open binding site trans to N7 is taken into account.

For the location of transition states, the synchronous transit-guided quasi-Newton (STQN) method, as implemented in Gaussian 03,[30] was used. The resulting optimized structures were verified as transition states by frequency calculations, and the single negative frequency was investigated using GaussView[31] to verify that the correct transition state was obtained.

With the described methodology and a fairly simple computational setup (rigid PES scans, varying the O···O distance in $H_2O_2$ and 2 •OH, zero-point and free energy corrections were not included),[35] the calculated bond length in isolated $H_2O_2$ is 1.456 Å, which is around 0.02 Å shorter than the experimentally determined value of 1.475 Å.[32] The H−O−O−H torsion angle of 118.68° is in good agreement with experiment (116.0°), and the O−O−H angles of 99.7° are reasonably close to the experimental value of 94.8°. The bond dissociation energy (BDE) for homolytic cleavage of the O−O bond in free $H_2O_2$ was calculated and compared to the experimental[33] and a previously published DFT value.[34] The experimental energy needed for breaking the O−O bond at 25 °C is 213 kJ/mol, and the BDE calculated in a previous

(21) Frisch, M. J.; Trucks, G. W.; Schlegel, H. B.; Scuseria, G. E.; Robb, M. A.; Cheeseman, J. R.; Montgomery, J. A., Jr.; Vreven, T.; Kudin, K. N.; Burant, J. C.; Millam, J. M.; Iyengar, S. S.; Tomasi, J.; Barone, V.; Mennucci, B.; Cossi, M.; Scalmani, G.; Rega, N.; Petersson, G. A.; Nakatsuji, H.; Hada, M.; Ehara, M.; Toyota, K.; Fukuda, R.; Hasegawa, J.; Ishida, M.; Nakajima, T.; Honda, Y.; Kitao, O.; Nakai, H.; Klene, M.; Li, X.; Knox, J. E.; Hratchian, H. P.; Cross, J. B.; Bakken, V.; Adamo, C.; Jaramillo, J.; Gomperts, R.; Stratmann, R. E.; Yazyev, O.; Austin, A. J.; Cammi, R.; Pomelli, C.; Ochterski, J. W.; Ayala, P. Y.; Morokuma, K.; Voth, G. A.; Salvador, P.; Dannenberg, J. J.; Zakrzewski, V. G.; Dapprich, S.; Daniels, A. D.; Strain, M. C.; Farkas, O.; Malick, D. K.; Rabuck, A. D.; Raghavachari, K.; Foresman, J. B.; Ortiz, J. V.; Cui, Q.; Baboul, A. G.; Clifford, S.; Cioslowski, J.; Stefanov, B. B.; Liu, G.; Liashenko, A.; Piskorz, P.; Komaromi, I.; Martin, R. L.; Fox, D. J.; Keith, T.; Al-Laham, M. A.; Peng, C. Y.; Nanayakkara, A.; Challacombe, M.; Gill, P. M. W.; Johnson, B.; Chen, W.; Wong, M. W.; Gonzalez, C.; Pople, J. A. *Gaussian 03*, revision B.03; Gaussian, Inc.: Wallingford, CT, 2004.
(22) Becke, A. D. *J. Chem. Phys. B* **1993**, *98*, 5648.
(23) Lee, C.; Yang, W.; Parr, R. G. *Phys. Rev. B* **1988**, *37*, 785.
(24) Cancès, M. T.; Mennucci, B.; Tomasi, J. *J. Chem. Phys.* **1997**, *107*, 3032.
(25) Cossi, M.; Barone, B.; Mennucci, B.; Tomasi, J. *Chem. Phys. Lett.* **1998**, *286*, 253.
(26) Mennucci, B.; Tomasi, J. *J. Chem. Phys.* **1997**, *106*, 5151.
(27) Cossi, M.; Scalmani, G.; Raga, N.; Barone, V. *J. Chem. Phys.* **2002**, *117*, 43.
(28) Schäfer, A.; Huber, C.; Ahlrichs, R. *J. Chem. Phys.* **1994**, *100*, 5829.
(29) Note that this is a computational simplification. Since no optimizations were performed at the TZVPP level, frequency calculations would be meaningless. While the difference in methods does introduce some error, this error is small in comparison to the total energy. The important point is that the relative free energy corrections must be consistent, which is the case.
(30) This method uses a linear synchronous transit or quadratic synchronous transit approach to get closer to the quadratic region around the transition state and then uses a quasi-Newton or eigenvector-following algorithm to complete the optimization. It is started with the keywords QST2 and QST3, where QST2 requires two molecule specifications (for the reactant and product) as its input, while QST3 requires three molecule specifications (for the reactant, the product, and an initial structure of the transition state).
(31) Dennington, R., II; Keith, T.; Milliam, J.; Eppinnett, K.; Hovell, W. L.; Gilliland, R. *GaussView*, version 3.09; Semichem, Inc.: Shawnee Mission, KS, 2003.
(32) Oelfke, W. C.; Gordy, W. *J. Chem. Phys.* **1969**, *51*, 5336.
(33) Solomons, T. W. G. *Organic Chemistry*, 5th ed.; Wiley: New York, 1992.
(34) Buda, F.; Ensing, B.; Gribnau, M. C. M.; Baerends, E. J. *Chem.—Eur. J.* **2001**, *7*, 2775.

**Table 1.** Selected Geometric Parameters of $[L^2Fe(NCCH_3)_2]^{2+}$ and $[L^5Fe(NCS)_2]$ Experimental Parameters Given in Italic

| complex parameters | $[L^2Fe(NCCH_3)_2]^{2+}$ $S=0$ | $[L^2Fe(NCCH_3)_2]^{2+}$ $S=2$ | $[L^2Fe(NCS)_2]$[14] $S=2$ |
|---|---|---|---|
| | Bond Distances (Å) | | |
| Fe−N7 | 2.210 | 2.385 | *2.373* |
| Fe−N3 | 2.031 | 2.241 | *2.242* |
| Fe−Npy1 | 2.004 | 2.172 | *2.170* |
| Fe−Npy2 | 2.004 | 2.170 | *2.176* |
| Fe−$N_E$[a] | 1.935 | 2.131 | *2.038* |
| Fe−$N_A$[a] | 1.938 | 2.234 | *2.117* |
| N3···N7 | 2.916 | 3.028 | *2.922* |
| | Valence Angles (deg) | | |
| N7−Fe−N3 | 86.78 | 81.70 | *78.52* |
| Npy1−Fe−Npy2 | 165.20 | 152.78 | *149.67* |

[a] $N_E$ refers to the nitrogen atom of the acetonitrile coordinated in the equatorial plane (trans to N3), while $N_A$ refers to the axially coordinated acetonitrile (trans to N7).

DFT study using the PW91 functional and a triple-$\xi$ basis set with one polarization function, as implemented in ADF, is 234 kJ/mol.[34] We calculate a value of 238 kJ/mol, 25 kJ/mol larger than experiment but in good agreement with the previously calculated DFT value.[34] This is an indication that the reaction energies and energy barriers are not strongly dependent on the DFT method (B3LYP vs PW91, double vs triple $\xi$ basis).

## Results and Discussion

**1. The $[L^2Fe^{II}(NCCH_3)_2]^{2+}$ Precursor and the Primary Intermediate $[L^2Fe^{II}(HOOH)(NCCH_3)]^{2+}$.** Calculations were performed on the $[L^2Fe^{II}(NCCH_3)_2]^{2+}$ precursor, and the results were compared to available experimental data. The geometry was optimized for the $S=0$ and $S=2$ spin states (convergence could not be reached for the $S=1$ state), and the high-spin ($S=2$) state is more stable, in agreement with experiment.[14] The singlet state is calculated to be 33.5 kJ/mol higher in energy than the quintet ground state. A Mulliken spin density of 3.80 results for the iron center in the ground state, in the expected region for a high-spin $d^6$ $Fe^{II}$ center (four unpaired electrons), with the remaining spin density shared among the donor atoms. Since no crystal structure has been obtained for $[L^2Fe^{II}(NCCH_3)_2]^{2+}$, the calculated structure was compared to the crystal structure of $[L^2Fe^{II}(SCN)_2]$. The correspondence is good, as can be seen from Table 1. The geometric parameters of the $\{L^2Fe\}$ fragment in $[L^2Fe^{II}(NCCH_3)_2]^{2+}$ are practically identical to those of $[L^2Fe^{II}(NCS)_2]$.

For all three reaction pathways (see Scheme 1), the first step is ligand exchange at the site trans to N3 to form $[L^2Fe^{II}(HOOH)(NCCH_3)]^{2+}$. This reaction is endothermic by 18.7 kJ/mol. The structure of the $[L^2Fe^{II}(HOOH)(NCCH_3)]^{2+}$ complex was optimized in all possible spin states, and a quintet ground state ($S=2$) is calculated (see Figure 1a). The singlet and triplet states are 68.0 and 70.8 kJ/mol higher, respectively.

Selected bond lengths and stretching frequencies, as well as the relative energies of the different spin states, are given in Table 2. The coordinates of the optimized geometries are given as Supporting Information. In all three spin states, hydrogen peroxide is monodentately coordinated to the iron center, as can be seen from the Fe···O2 distances. The O−O bond length in the quintet ground state is 1.452 Å, which is only slightly shorter than the value of 1.456 Å calculated for uncoordinated $H_2O_2$. However, the O−O stretching frequency is lowered from 939 $cm^{-1}$ in $H_2O_2$ to 911 $cm^{-1}$ in $[L^2Fe^{II}(HOOH)(NCCH_3)]^{2+}$, which indicates a weakening of the O−O bond upon coordination to the iron center. The Mulliken spin density of 3.79 on the iron center is similar to that in $[L^2Fe^{II}(NCCH_3)_2]^{2+}$, indicating that there is minimal charge transfer to the $H_2O_2$ ligand.

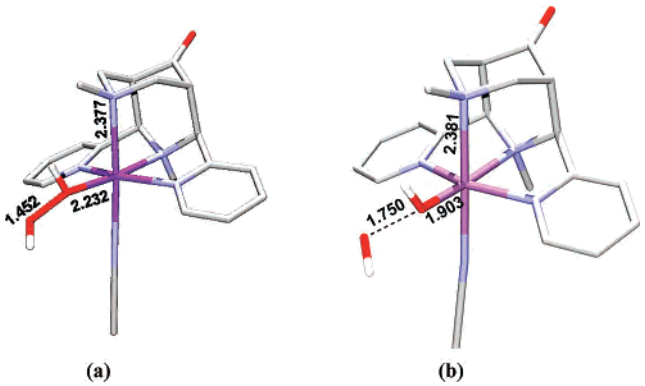


**Figure 1.** (a) Optimized geometry of the primary intermediate $[L^2Fe^{II}(HOOH)(NCCH_3)]^{2+}$ in its high-spin ($S=2$) ground state; (b) optimized geometry of the transition state for the homolytic cleavage of $[L^2Fe^{II}(HOOH)(NCCH_3)]^{2+}$ in its high-spin ($S=2$) ground state.

**Table 2.** Selected Geometric Parameters, Stretching Frequencies, and Relative Energies of the Spin States in the $Fe^{II}$-hydrogen Peroxide Complexes of $L^2$

| | interatomic distances (Å) | | | | |
|---|---|---|---|---|---|
| | Fe−O1 | Fe−O2 | O1−O2 | $\nu$ ($cm^{-1}$) O1−O2 | $\Delta G$ (kJ/mol) 295.15 K |
| | | | $[L^2Fe^{II}(NCCH_3)(HOOH)]^{2+}$ | | |
| $S=0$ | 2.067 | 3.065 | 1.462 | 860 | 68.0 |
| $S=1$ | 2.157 | 3.156 | 1.457 | 889 | 70.8 |
| $S=2$ | 2.232 | 3.173 | 1.452 | 911 | 0.0 |
| | | | $[L^2Fe^{II}(HOOH)]^{2+}$ | | |
| $S=0$ | 2.204 | 2.147 | 1.455 | 930 | 80.0 |
| $S=1$ | 2.005 | 2.818 | 1.468 | 837 | 53.6 |
| $S=2$ | 2.216 | 2.878 | 1.454 | 918 | 0.0 |
| | | | $[L^2Fe^{II}(OH_2)(HOOH)]^{2+}$ | | |
| $S=0$ | 2.077 | 3.040 | 1.473 | 800 | 79.0 |
| $S=1$ | 2.040 | 3.063 | 1.479 | 759 | 76.4 |
| $S=2$ | 2.349 | 3.298 | 1.456 | 898 | 0.0 |

Since a small amount of water is present in the reaction mixture of the catalytic experiments, ligand exchange of the coordinated acetonitrile with water to form $[L^2Fe^{II}(HOOH)(OH_2)]^{2+}$ is possible. This reaction is calculated to be approximately thermoneutral (1.4 kJ/mol) but, since ligand exchange reactions in high-spin $Fe^{II}$ complexes generally follow dissociative reaction mechanisms,[36] should proceed via a pentacoordinate $[L^2Fe^{II}(HOOH)]^{2+}$ intermediate, the formation of which is exothermic by −18.5 kJ/mol.

(35) Zero-point corrections cannot be computed if a rigid PES scan is performed, since the structures are not fully optimized at each step of the scan and frequency calculations are meaningless unless the structure is fully optimized. Full optimizations at each point were considered unnecessary, since the exact energy has already been calculated and the point was simply to ascertain whether our results were consistent with this previously calculated value.

(36) van Eldik, R., Ed. *Inorganic High Pressure Chemistry*; Studies in Inorganic Chemistry, Vol. 7; Elsevier: Amsterdam and New York, 1986.

The structures of $[L^2Fe^{II}(HOOH)(OH_2)]^{2+}$ and $[L^2Fe^{II}(HOOH)]^{2+}$ were optimized in all possible spin states, and both have quintet ($S = 2$) ground states. The relative energies of the singlet and triplet states for these two complexes are also given in Table 2. Coordination of hydrogen peroxide to the iron center is $\eta^1$ in all cases except that of singlet $[L^2Fe^{II}(HOOH)]^{2+}$, and this can be rationalized in terms of ligand field theory. We define the coordinate system such that the Fe−N7 bond lies along the *z*-axis, the Fe−Npy bonds lie along the *x*-axis, and the Fe−N3 bond lies along the *y*-axis. Low-spin ($S = 0$) $Fe^{II}$ has a $(t_{2g})^6(e_g)^0$ configuration; the two $e_g$ orbitals are unoccupied, which makes coordination to vacant sites possible. In $[L^2Fe^{II}(HOOH)(NCCH_3)]^{2+}$ and $[L^2Fe^{II}(HOOH)(OH_2)]^{2+}$, the second coordination site is occupied, and in $[L^2Fe^{II}(HOOH)]^{2+}$ it is free for the coordination of the second oxygen atom from hydrogen peroxide. In the intermediate- and high-spin states, one ($S = 1$) or both ($S = 2$) of these orbitals are singly occupied, and $H_2O_2$ coordinates as a monodentate ligand in the direction of the empty or singly occupied $d_{x^2-y^2}$ orbital (trans to N3), regardless of whether an additional coligand is coordinated or not.

In the $S = 2$ ground state of $[L^2Fe^{II}(HOOH)]^{2+}$, the O−O stretching frequency is 918 $cm^{-1}$, which is lowered to 837 $cm^{-1}$ in the $S = 1$ state, indicating a weakening of the O−O bond. This is also reflected in O−O bond lengths, which increase from 1.453 Å ($S = 2$) to 1.468 Å ($S = 1$), while the Fe−O bond lengths decrease correspondingly from 2.216 Å ($S = 2$) to 2.005 Å ($S = 1$). The $S = 1$ state is therefore activated for bond cleavage with respect to the $S = 2$ ground state.

**2. The $Fe^{III}$-hydroperoxo−$Fe^{V}$-oxo-hydroxo Pathway (A).** The first reaction path considered (A in Scheme 1) can be divided into four steps: (i) O−O bond cleavage in the primary intermediate $[L^2Fe^{II}(HOOH)(NCCH_3)]^{2+}$ to form an $Fe^{III}$-hydroxo intermediate, $[L^2Fe^{III}(OH)(NCCH_3)]^{2+}$, (ii) reaction of $[L^2Fe^{III}(OH)(NCCH_3)]^{2+}$ with a second molecule of $H_2O_2$ to form $[L^2Fe^{III}(OOH)(NCCH_3)]^{2+}$ and $H_2O$, (iii) dissociation of acetonitrile in $[Fe^{III}L^2(OOH)(NCCH_3)]^{2+}$ to form $[L^2Fe^{III}(OOH)]^{2+}$, and (iv) O−O bond cleavage to form an $Fe^{V}$-oxo-hydroxo complex, $[L^2Fe^{V}{=}O(OH)]^{2+}$. Formation of an $Fe^{III}$-hydroxo intermediate and its reaction to an $Fe^{III}$-hydroperoxo product has been spectroscopically observed for pentadentate ligands, such as the pentadentate tpa derivative N4py,[37] $L^3$, and $L^4$.[15] Note that steps iii and iv have been assumed to be independent reactions for computational purposes (i.e., a dissociative mechanism is assumed), whereas in reality they will not be independent, since ligand exchange reactions in $Fe^{III}$ complexes are generally associative in nature.[36] The possibility of homolytic cleavage of the O−O bond in $[L^2Fe^{III}(OOH)(NCCH_3)]^{2+}$ to form $[L^2Fe^{IV}{=}O(NCCH_3)]^{2+}$ and an $^{\bullet}OH$ radical, a reaction which is postulated to take place for $L^3$ and $L^4$, is also discussed (in Scheme 1 species II in path A to species IV in path B).

The formation of an $Fe^{III}$-hydroxo intermediate may proceed directly via homolytic cleavage of the O−O bond in $[L^2Fe^{II}(HOOH)(NCCH_3)]^{2+}$ to form $[L^2Fe^{III}(OH)(NCCH_3)]^{2+}$ and an $^{\bullet}OH$ radical (eq 1) or via the reaction of $[L^2Fe^{II}(HOOH)(NCCH_3)]^{2+}$ with a second molecule of $[L^2Fe^{II}(NCCH_3)_2]^{2+}$ to form a dinuclear complex, which subsequently undergoes homolytic cleavage of the O−O bond to form two $[L^2Fe^{III}(OH)(NCCH_3)]^{2+}$ units (eq 2).

$$[L^2Fe^{II}(HOOH)(NCCH_3)]^{2+} \rightarrow [L^2Fe^{III}(OH)(NCCH_3)]^{2+} + {}^{\bullet}OH \quad (1)$$

$$[L^2Fe^{II}(HOOH)(NCCH_3)]^{2+} + [L^2Fe^{II}(NCCH_3)_2]^{2+} \rightarrow 2[L^2Fe^{III}(OH)(NCCH_3)]^{2+} + CH_3CN \quad (2)$$

The total reaction energy of direct homolytic cleavage in $[L^2Fe^{II}(HOOH)(NCCH_3)]^{2+}$ (eq 1) is −29.7 kJ/mol, and the energy barrier is calculated to be 60.7 kJ/mol in the gas phase. The optimized structure of the transition state is shown in Figure 1b. The O−O bond length in the transition state is increased to 1.750 Å, while the Fe−O bond length is decreased to 1.903 Å.

The total enthalpy of formation via a bimetallic transition state (eq 2) is −115.2 kJ/mol per unit of reactant. Due to the size of the system, no attempt to optimize the bimetallic transition state was made, so the height of the energy barrier for this reaction is unknown. However, the relatively low concentration of the $Fe^{II}$ catalyst in the reaction mixtures makes it improbable that the $[L^2Fe^{II}(HOOH)(NCCH_3)]^{2+}$ complex will react with a further $[L^2Fe^{II}(NCCH_3)_2]^{2+}$ species before a number of alternative reactions take place (see pathways B and C in Scheme 1). In addition, even if the enthalpy of formation of the dinuclear complex should be favorable, this is counterbalanced to some extent by a large, unfavorable entropy term.

Note that the hydroxyl radical formed by O−O homolysis in $[L^2Fe^{II}(HOOH)(NCCH_3)]^{2+}$ is also an oxidant, capable of oxidizing a second equivalent of the Fe(II) precursor complex. If this secondary reaction is taken into account, the same total enthalpy of formation is obtained as for the reaction via the bimetallic transition state (−115.2 kJ/mol), since the end products are the same. However, for the purpose of comparing possible reaction pathways, this secondary reaction is not accounted for in our analysis, since it is the reaction energy and activation barrier of the initial bond cleavage reaction which will determine which of the pathways is followed.

The geometry of $[L^2Fe^{III}(OH)(NCCH_3)]^{2+}$ was optimized for all possible spin states, and a high-spin ($S = {}^5/_2$) ground state with an Fe−O bond length of 1.770 Å is calculated to be the most favorable configuration. The $S = {}^3/_2$ and $S = {}^1/_2$ states are 35.6 and 42.7 kJ/mol higher in energy than the ground state with Fe−O bond lengths of 1.775 Å and 1.783 Å, respectively. The Fe−O bond lengths are shortened by approximately 0.02−0.03 Å relative to $[L^2Fe^{II}(HOOH)(NCCH_3)]^{2+}$.

The formation of $[L^2Fe^{III}(OOH)(NCCH_3)]^{2+}$ from $[L^2Fe^{III}(OH)(NCCH_3)]^{2+}$ via ligand exchange is calculated to be

(37) Roelfes, G.; Lubben, M.; Chen, K.; Ho, R. Y. N.; Meetsma, A.; Genseberger, S.; Hermant, R. M.; Hage, R.; Mandal, S. K.; Young, V. G., Jr.; Zang, Y.; Kooijman, H.; Spek, A. L.; Que, L., Jr.; Feringa, B. L. *Inorg. Chem.* **1999**, *38*, 1929.

**Table 3.** Fe−O and O−O Bond Distances and Frequencies in the $Fe^{III}$-hydroperoxo Complexes of $L^2$

| | bond length (Å) | | | $\Delta E$ (kJ/mol) | | |
|---|---|---|---|---|---|---|
| | Fe−O1 | O1−O2 | $\nu$ ($cm^{-1}$) O1−O2 | 0 K[a] | 298.15 K[b] | $\Delta G$ (kJ/mol) 298.15 K[c] |
| | | | $[L^2Fe^{III}(NCCH_3)(OOH)]^{2+}$ | | | |
| $S = 1/2$ | 1.775 | 1.442 | 890 | 2.3 | 0.0 | 15.9 |
| $S = 3/2$ | 1.777 | 1.438 | 918 | 12.4 | 14.1 | 13.5 |
| $S = 5/2$ | 1.852 | 1.414 | 940 | 0.0 | 2.9 | 0.0 |
| | | | $[L^2Fe^{III}(OOH)]^{2+}$ | | | |
| $S = 1/2$ | 1.804 | 1.462 | 888 | 9.5 | 5.8 | 23.5 |
| $S = 3/2$ | 1.760 | 1.450 | 877 | 0.0 | 0.0 | 4.4 |
| $S = 5/2$ | 1.829 | 1.416 | 933 | 0.9 | 2.4 | 0.0 |
| | | | $[L^2Fe^{III}(OH_2)(OOH)]^{2+}$ | | | |
| $S = 1/2$ | 1.790 | 1.460 | 866 | 10.9 | 5.6 | 22.8 |
| $S = 3/2$ | 1.784 | 1.450 | 894 | 12.6 | 11.3 | 16.3 |
| $S = 5/2$ | 1.862 | 1.428 | 936 | 0.0 | 0.0 | 0.0 |

[a] Zero-point corrections included. [b] Zero-point and thermal corrections included. [c] Zero-point, thermal, and entropy corrections included.

endothermic by +11.3 kJ/mol. Removal of the $CH_3CN$ coordinated trans to N7 to form the pentacoordinate $[L^2Fe^{III}(OOH)]^{2+}$ complex is exothermic by −33.1 kJ/mol, and ligand exchange to form $[L^2Fe^{III}(OOH)(OH_2)]^{2+}$ has a reaction energy of 9.4 kJ/mol.

The relative energies of all spin states of the $Fe^{III}$-hydroperoxo complexes are given in Table 3, along with selected bond lengths and the O−O stretching frequencies. In acetonitrile, the $[L^2Fe^{III}(OOH)(NCCH_3)]^{2+}$ complex is predicted to have a high-spin ($S = 5/2$) ground state at 298.15 K (zero-point and free energy corrections included), the low-spin ($S = 1/2$) state lies 15.9 kJ/mol and the intermediate-spin ($S = 3/2$) state lies 13.5 kJ/mol higher in energy. For the pentacoordinate $[L^2Fe^{III}(OOH)]^{2+}$ complex, the $S = 3/2$ and $S = 5/2$ states are low in energy and very close lying, and the low-spin ($S = 1/2$) state has an energy of 23.5 kJ/mol relative to the ground state. The ground state of $[L^2Fe^{III}(OOH)(OH_2)]^{2+}$ is also high-spin ($S = 5/2$), and the destabilization of the $S = 3/2$ and $S = 1/2$ states with respect to the ground state are 16.3 and 22.9 kJ/mol, respectively. From the computed energies, it emerges that the spin states are quite close in energy, and the ground state depends on the solvent and temperature. This also follows from experiment, since the $[L^2Fe^{III}(OO^tBu)]^{2+}$ complex lies close to the spin-crossover limit, and a spin state flip can be induced by a change of temperature and/or solvent.[17]

Homolytic cleavage of the O−O bond in $[L^2Fe^{III}(OOH)(NCCH_3)]^{2+}$ leads to the formation of $[L^2Fe^{IV}{=}O(NCCH_3)]^{2+}$ and an •OH radical. This reaction is calculated to be endothermic by 42.1 kJ/mol which is highly unfavorable, and a similar strongly endothermic reaction has also been proposed due to the calculated reaction energy of the analogous reaction in bleomycin[7] and for the reaction of $[(tpa)Fe^{III}(OOH)(OH_2)]^{2+}$ to $[(tpa)Fe^{IV}(O)(OH_2)]^{2+}$, which has a reaction energy of 79 kJ/mol.[38]

The product of O−O bond cleavage in $[L^2Fe^{III}(OOH)]^{2+}$ is a $[L^2Fe^{V}{=}O(OH)]^{2+}$ complex, in which the formed •OH radical is immediately trapped by the iron center. This

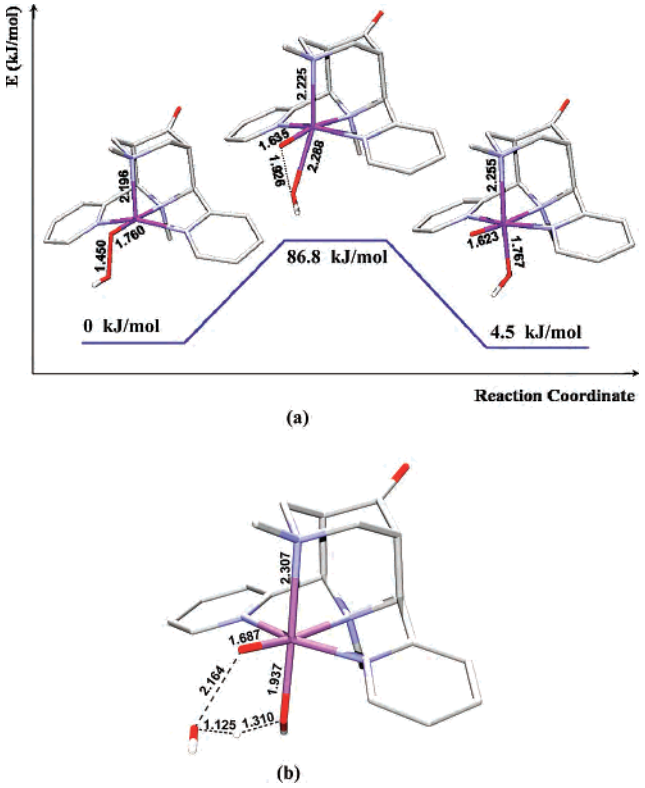


**Figure 2.** (a) The reactant, transition state, and product of heterolytic cleavage in $[L^2Fe^{III}(OOH)]^{2+}$ on the $S = 3/2$ surface; (b) the optimized geometry of the transition state in the water-assisted pathway.

reaction is slightly endothermic (4.5 kJ/mol) and has an energy barrier of 86.8 kJ/mol. Figure 2a shows the calculated structures of the reactant, transition state, and product of this reaction, including relevant bond lengths and relative energies.

The Fe−O bond length decreases from 1.760 Å in the reactant to 1.635 Å in the transition state, indicating that the Fe−O bond already has significant double-bond character in the transition state. This is supported by the calculated spin density of 0.37 on the iron-bound oxygen atom, which indicates a delocalization of spin density to the iron center, due to the formation of the double bond. The spin density of −0.63 on the oxygen atom of the resulting •OH unit is indicative of radical formation, which implies that the O−O bond cleavage takes place homolytically.

The geometry of $[L^2Fe^{V}{=}O(OH)]^{2+}$ was optimized for both the $S = 1/2$ and $S = 3/2$ spin states. The ground spin state is the same as that of $[L^2Fe^{III}(OOH)]^{2+}$ ($S = 3/2$), which implies that the reaction will be facilitated by the dissociation of $CH_3CN$ in $[L^2Fe^{III}(OOH)(NCCH_3)]^{2+}$, which does not have a quartet ground state. In addition, the near degeneracy of the $S = 1/2$ and $S = 5/2$ spin states of $[L^2Fe^{III}(OOH)(NCCH_3)]^{2+}$ and the $S = 5/2$ and $S = 3/2$ spin states of $[L^2Fe^{III}(OOH)]^{2+}$ should facilitate the spin-state-crossover required prior to cleavage of the O−O bond.

The Fe−O bond distance in the ground state of $[L^2Fe^{V}{=}O(OH)]^{2+}$ is 1.623 Å, which is around 0.040 Å shorter than the corresponding bond length calculated for the $[(tpa)Fe^{V}{=}O(OH)]^{2+}$ complex (1.665 Å).[38] This difference is large enough to be considered significant, despite the fact that the

(38) Bassan, A.; Blomberg, M. R. A.; Siegbahn, P. E. M.; Que, L., Jr. *J. Am. Chem. Soc.* **2002**, *124*, 11056.

**Scheme 2**

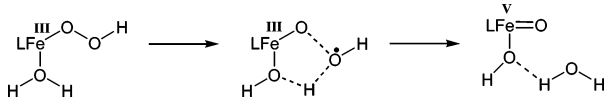

use of different methodologies may also be a contributing factor. It is therefore likely that $L^2$ does induce shorter bond lengths than tpa, due to the strong in-plane binding trans to the tertiary amine donor N3.

Although high-spin $Fe^V$ normally has three unpaired electrons, one expects a spin density on iron of around 2, due to the delocalization of two unpaired electrons in the two Fe=O $\pi^*$ orbitals.[39] Indeed, a spin density of 2.07 is calculated on the iron center, with the bulk of the remaining spin density on the oxo ligand (0.87) and a small amount on the oxygen of the hydroxy ligand (0.16).

In analogy to the reactions discussed below for $[L^2Fe^{II}(HOOH)(OH_2)]^{2+}$ and $[L^2Fe^{II}(OOH)(OH_2)]^{+}$, there is the possibility of a "water-assisted" pathway for the formation of $[L^2Fe^{V}{=}O(OH)]^{2+}$ from $[L^2Fe^{III}(OOH)(OH_2)]^{2+}$, following ligand exchange of $CH_3CN$ with $H_2O$ trans to N7 as schematically shown in Scheme 2. This is the proposed mechanism of oxidation with the tetradentate ligand tpa.[38]

The transition state has been calculated for the spin ground state of the $[L^2Fe^{III}(OOH)(OH_2)]^{2+}$ species, and the calculated barrier is 141.0 kJ/mol. This reaction is slightly exothermic with the reaction energy of 4.8 kJ/mol. Figure 2b shows the calculated structure of the transition state including the relevant bond lengths.

In summary, due to the high barrier calculated for the conversion of $[L^2Fe^{II}(HOOH)(NCCH_3)]^{2+}$ to $[L^2Fe^{III}(OH)(NCCH_3)]^{2+}$ (79.4 kJ/mol) and from $[L^2Fe^{III}(OOH)]^{2+}$ to $[L^2Fe^{V}{=}O(OH)]^{2+}$ (86.8 kJ/mol, without water; 150.4, water-assisted) and higher overall reaction energies compared to the favorable $Fe^{II}/Fe^{IV}$ alternatives discussed below, O−O bond cleavage in $[L^2Fe^{III}(OOH)(NCCH_3)]^{2+}$ to form $[L^2Fe^{V}{=}O(OH)]^{2+}$, proposed to be the reactive intermediate in the oxidation of olefins with tpa,[38,40] is less likely to take place in our bispidine-based system.

**3. The $Fe^{IV}$-dihydroxo−$Fe^{IV}$-oxo-aqua Pathway (B).** The second reaction mechanism (B in Scheme 1) can also be divided into four steps: (i) dissociation of acetonitrile in the primary intermediate $[L^2Fe^{II}(HOOH)(NCCH_3)]^{2+}$, (ii) cleavage of the O−O bond in $[L^2Fe^{II}(HOOH)]^{2+}$ to form an $Fe^{IV}$-dihydroxo intermediate, $[L^2Fe^{IV}(OH)_2]^{2+}$, (iii) proton transfer from the trans to N3 to the trans to N7 bound hydroxide of $[L^2Fe^{IV}(OH)_2]^{2+}$ to form $[L^2Fe^{IV}{=}O(OH_2)]^{2+}$, and (iv) ligand exchange to form $[L^2Fe^{IV}{=}O(NCCH_3)]^{2+}$. Note that, as for the reaction of $[L^2Fe^{III}(OOH)(NCCH_3)]^{2+}$ to $[L^2Fe^{V}{=}O(OH)]^{2+}$, a dissociative mechanism is assumed, and steps i and ii are considered separately. Since ligand exchange reactions in high-spin $Fe^{II}$ complexes are generally dissociative in nature,[36] the computational simplification is justified in this case. Not shown in Scheme 1 but also discussed here is the possibility of ligand exchange of acetonitrile with water in $[L^2Fe^{II}(HOOH)(NCCH_3)]^{2+}$, followed by homolytic cleavage of the O−O bond in the $[L^2Fe^{II}(HOOH)(OH_2)]^{2+}$ complex to form $[L^2Fe^{IV}(OH)_2]^{2+}$ and water.

As discussed above, the formation of $[L^2Fe^{IV}(OH)_2]^{2+}$ from $[L^2Fe^{II}(HOOH)(NCCH_3)]^{2+}$ can be divided into two parts, i.e., dissociation of the $CH_3CN$ molecule bound trans to N7 to form a pentacoordinated $[L^2Fe^{II}(HOOH)]^{2+}$ species with a free coordination site, followed by O−O bond heterolysis in $[L^2Fe^{II}(HOOH)]^{2+}$. The dissociation of acetonitrile is exothermic by 18.5 kJ/mol (see above) and the formation of $[L^2Fe^{IV}(OH)_2]^{2+}$ from $[L^2Fe^{II}(HOOH)]^{2+}$ is exothermic by 76.7 kJ/mol, bringing the total energy of the reaction (eq 3) to −95.2 kJ/mol.

$$[L^2Fe^{II}(HOOH)(NCCH_3)]^{2+} \rightarrow [L^2Fe^{IV}(OH)_2]^{2+} + CH_3CN \quad (3)$$

The ground state of $[L^2Fe^{IV}(OH)_2]^{2+}$ is calculated to have an $S = 1$ configuration, by a margin of 4.5 kJ/mol with respect to the high-spin ($S = 2$) state. The $S = 0$ state lies 100.0 kJ/mol higher in energy than the ground state. Because the reactant and product of O−O bond cleavage have different spin states, a spin-forbidden transition from the quintet to the triplet state must take place somewhere along the reaction path, and both spin state surfaces are considered. The geometries of the reactants, transition states, and products of the reaction of $[L^2Fe^{II}(HOOH)]^{2+}$ to $[L^2Fe^{IV}(OH)_2]^{2+}$ for both $S = 1$ and $S = 2$ configurations, including relevant bond lengths and relative energies, are shown in Figure 3.

Investigation of the potential energy surfaces for the $S = 1$ and $S = 2$ states reveals that the transition states are very close in energy, despite having very different geometries. Apart from the obvious shortening of the Fe−O1 and lengthening of the O1−O2 bond (where O1 is the oxygen atom bound to the iron center and O2 is the second oxygen atom of $H_2O_2$), the geometry of the triplet transition state is very similar to that of the reactant. The Fe−N7 bond lengths are identical, the Fe−O1−O2 angle is hardly changed (from 107.5° in the reactant to 105.2° in the transition state), and formation of the Fe−O2 bond has not yet started. This is in agreement with the low-energy barrier of 29.2 kJ/mol. However, since the triplet state of the reactant is destabilized by 53.6 kJ/mol relative to the quintet ground state (see Table 2 and Figure 3), the transition state on the triplet surface lies 82.8 kJ/mol higher in energy than the quintet ground state of $[L^2Fe^{II}(HOOH)]^{2+}$.

The transition state on the quintet surface is 81.8 kJ/mol higher in energy than the reactant and is only 1 kJ/mol lower in energy than the triplet transition state (Figure 3). In keeping with the higher energy barrier, the geometry of the transition state on the quintet surface is closer to that of the product than in the triplet state. The Fe−O1−O2 angle has decreased from 101.3° in the reactant to 71.7° in the transition state; the Fe−N7 bond is slightly lengthened, the Fe−O2 bond is already formed, and the O−O bond is

(39) Shaik, S.; Filatov, M.; Schröder, D.; Schwarz, H. *Chem.—Eur. J.* **1998**, *4*, 193.
(40) Bassan, A.; Blomberg, M. R. A.; Siegbahn, P. E. M.; Que, L., Jr. *Chem.—Eur. J.* **2005**, *11*, 692.

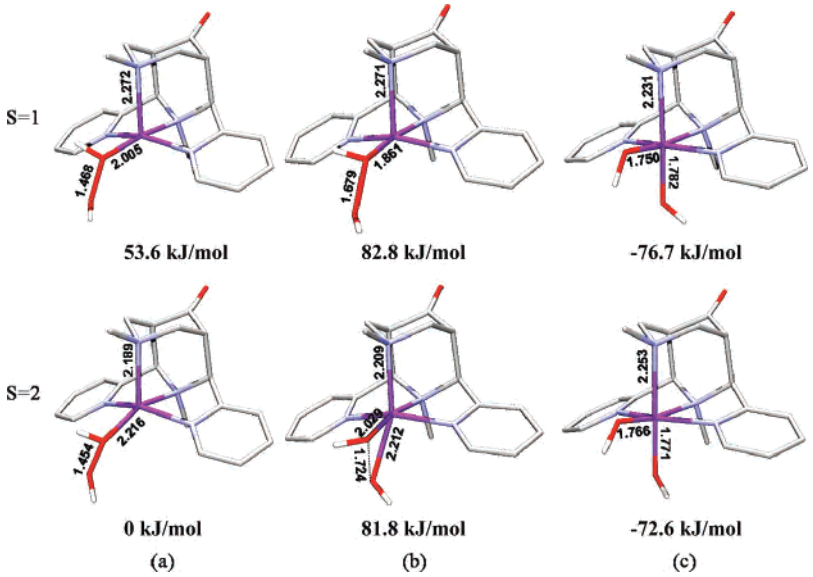


**Figure 3.** The reactant (a), transition state (b), and product (c) of heterolytic O−O bond cleavage in $[L^2Fe^{II}(HOOH)]^{2+}$ for $S = 1$ and $S = 2$.

**Scheme 3**

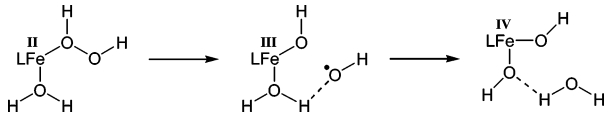

elongated. From the large energy difference between the $S = 1$ and $S = 2$ states of the reactant, an early spin-state-crossover can be excluded, while the near degeneracy of transition states on the triplet and quintet surfaces strongly suggests that the spin-flip takes place after the transition state is reached. We have not attempted to calculate the minimum energy crossing points (MECP) between the two surfaces.[41,42] Coordination of hydrogen peroxide to the $FeL^2$ fragment therefore greatly reduces the energy required to cleave the O−O bond, from ~240 kJ/mol in free $H_2O_2$ to 81.8 kJ/mol in $[L^2Fe^{II}(HOOH)]^{2+}$. This is in agreement with the observed weakening of the O−O bond in coordinated $H_2O_2$, as discussed above.

Both in the $S = 1$ and in the $S = 2$ transition states, the oxygen atom of the formed •OH radical has significant spin density in the transition state (−0.31 and 0.30 for $S = 1$ and $S = 2$, respectively), indicating that the O−O bond cleavage takes place homolytically, as for $[L^2Fe^{III}(OOH)]^{2+}$. Since no Fe−O double bond is formed in this case, the iron-bound oxygen atoms, on the other hand, have practically no spin density (0.00 and 0.01 for $S = 1$ and $S = 2$).

Another possibility for formation of $[L^2Fe^{IV}(OH)_2]^{2+}$ is a "water-assisted" mechanism such as that postulated for $[(H_2O)_5Fe^{II}(HOOH)]^{2+}$.[34] For our system, this involves ligand exchange of $CH_3CN$ with $H_2O$ to form $[L^2Fe^{II}(HOOH)(OH_2)]^{2+}$, followed by the formation of a short-lived $[L^2Fe^{III}(OH_2)(OH)]^{2+}$ species and an •OH radical, which immediately abstracts a hydrogen atom from the trans to N7 bound $H_2O$ molecule, forming the $[L^2Fe^{IV}(OH)_2]^{2+}$ final product and a water molecule hydrogen bonded to the trans

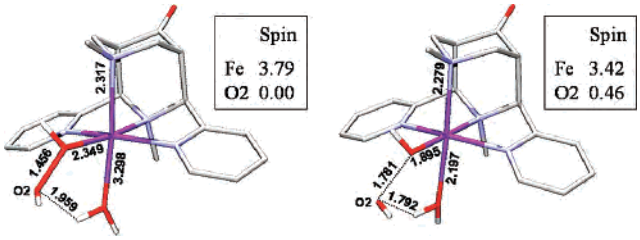


**Figure 4.** The reactant and transition state for homolytic cleavage in $S = 2$ $[L^2Fe^{II}(HOOH)(OH_2)]^{2+}$, showing the Mulliken spin densities on Fe and O2.

to N7 bound hydroxyl ligand. This is shown schematically in Scheme 3.

As discussed previously, the thermoneutral ligand exchange proceeds via a pseudo-pentacoordinate intermediate and has a reaction energy of −18.5 kJ/mol. Since the ground state of the $[L^2Fe^{II}(HOOH)(OH_2)]^{2+}$ complex has an $S = 2$ electronic configuration, this reaction again involves a forbidden spin-state-crossover. The transition state for O−O bond cleavage on the high-spin ($S = 2$) surface has an energy of 74.5 kJ/mol relative to the $S = 2$ ground state of the reactant, which is somewhat lower than the energy of the $S = 1$ reactant (76.3 kJ/mol). The energy barrier on the $S = 1$ surface is only 18.1 kJ/mol, but the transition state has an energy of 94.4 kJ/mol with respect to the $S = 2$ ground state. This indicates that the O−O bond cleavage will take place on the quintet surface and that the spin-crossover occurs after the transition state has been formed. The reaction energy for the conversion of $[L^2Fe^{II}(HOOH)(OH_2)]^{2+}$ to $[L^2Fe^{IV}(OH)_2]^{2+}\cdot H_2O$ is highly exothermic by 143.7 kJ/mol.

The geometries of the quintet reactant and transition states are shown in Figure 4. The Fe−O1 bond length is decreased from 2.349 Å in the reactant to 1.895 Å in the transition state, and the O1−O2 distance increases from 1.456 to 1.781 Å. The $Fe^{III}$ intermediate and the second transition state were not optimized, since the reaction is analogous to the formation of $[L^2Fe^{IV}{=}O(OH)]^+$ from $[L^2Fe^{II}(OOH)(OH_2)]^+$ (see below), for which the energy barrier of the proton-

(41) Harvey, J. N.; Aschi, M. *Faraday Discuss.* **2003**, *124*, 129.
(42) Harvey, J. N. *Faraday Discuss.* **2004**, *127*, 165.

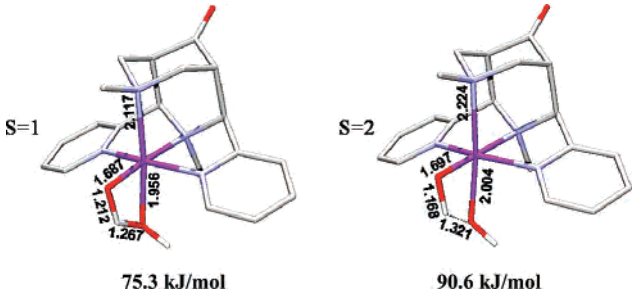


**Figure 5.** Transition states for the reaction of $[L^2Fe^{IV}(OH)_2]^{2+}$ to $[L^2Fe^{IV}(O)(OH_2)]^{2+}$ for $S = 1$ and $S = 2$.

**Scheme 4**

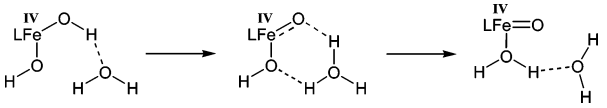

transfer step is shown to be negligible in comparison to that of O−O bond cleavage. Also shown in Figure 4 are the spin densities on Fe and O2 in the quintet reactant and transition states. In the reactant, the spin density on Fe is 3.79, as one would expect for high-spin $Fe^{II}$ ($d^6$, four unpaired electrons), and there is no net spin density on O2. In the transition state, the spin density on iron decreases to 3.42 and there is a net spin density of 0.46 on O2, indicating a transition to an $Fe^{III}$ intermediate ($d^5$, three unpaired electrons) and an •OH radical.

The energy barrier of 74.5 kJ/mol is comparable to the energy barrier of 81.8 kJ/mol for O−O bond cleavage in $[L^2Fe^{II}(HOOH)]^{2+}$. Since the energy barrier for the ligand exchange of $CH_3CN$ with $H_2O$ is also low, the main factor determining which pathway is followed will be the relative concentrations of $CH_3CN$ and $H_2O$. Under the catalytic conditions (oxidation of alkenes by $H_2O_2$ in $CH_3CN$), direct O−O bond cleavage in $[L^2Fe^{II}(HOOH)]^{2+}$ should take place almost exclusively.

Proton transfer from the trans to N3 to the trans to N7 bound hydroxide of $[L^2Fe^{IV}(OH)_2]^{2+}$ leads to the formation of an $[L^2Fe^{IV}{=}O(OH_2)]^{2+}$ complex. The geometry of this species was optimized for the $S = 1$ and $S = 2$ states, and the quintet state is calculated to be 22.4 kJ/mol more stable than the triplet state. The total energy of the reaction (eq 4) is −23.2 kJ/mol.

$$[L^2Fe^{IV}(OH)_2]^{2+} \rightarrow [L^2Fe^{IV}(O)(OH_2)]^{2+} \qquad (4)$$

Since $[L^2Fe^{IV}(OH)_2]^{2+}$ has a triplet ground state, this reaction again involves a forbidden spin-state-crossover, and both the $S = 1$ and $S = 2$ pathways were considered. The activation barrier on the $S = 2$ surface is 86.5 kJ/mol, bringing the total energy of the quintet transition state to 90.6 kJ/mol with respect to the triplet ground state of $[L^2Fe^{IV}(OH)_2]^{2+}$. The $S = 1$ transition state, on the other hand, lies 75.3 kJ/mol higher in energy than the reactant and is the more likely pathway. The spin-crossover is therefore expected to take place close to or in the product state. Figure 5 shows the geometries of the transition states and energies for both the $S = 1$ and $S = 2$ states relative to the ground state of $[L^2Fe^{IV}(OH)_2]^{2+}$. Unlike the transition states for the

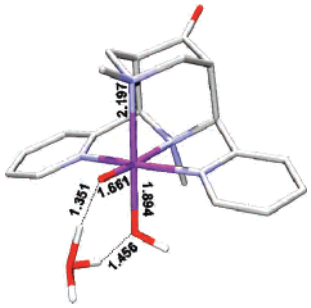


**Figure 6.** The transition state on the $S = 1$ surface for the water-assisted proton-transfer reaction of $[L^2Fe^{IV}(OH)_2]^{2+}$ to $[L^2Fe^{IV}{=}O(OH_2)]^{2+}$.

O−O homolysis, the geometries of the transition states for the proton transfer are similar for the $S = 1$ and $S = 2$ pathways.

An alternative to the direct proton transfer in $[L^2Fe^{IV}(OH)_2]^{2+}$ is a "water-assisted" mechanism, where a $H_2O$ molecule in the second coordination sphere acts as a proton shuffle, abstracting a proton from the trans to N3 bound hydroxide and transferring one to the second, trans to N7 bound hydroxide. This is shown schematically in Scheme 4.

One expects this reaction to be more favorable than direct proton transfer, due to the fact that a five-membered ring is formed in the transition state, instead of the strained four-membered ring in the transition state of the direct proton-transfer reaction. Indeed, the energy barrier on the $S = 1$ surface is lowered from 75.3 kJ/mol in the direct reaction to only 34.7 kJ/mol in the water-assisted mechanism. The $S = 2$ transition state was not optimized, since we have shown that the spin-state-crossover is likely to take place in the $Fe^{IV}{=}O$ product and because the spin state of the metal is unlikely to affect the energy barrier of a proton-transfer reaction. The reaction energy for the conversion from $[L^2Fe^{IV}(OH)_2]^{2+}{\cdot}H_2O$ to $[L^2Fe^{IV}{=}O(OH_2)]^{2+}{\cdots}OH_2$ is exothermic by −18.5 kJ/mol. Figure 6 shows the geometry of the transition state on the triplet surface. The Fe−O1 bond length in the water-assisted transition state is 1.661 Å, slightly shorter from the 1.687 Å found in the direct proton-transfer transition state in the triplet state.

**4. The $Fe^{II}$-hydroperoxo−$Fe^{IV}$-oxo-hydroxo Pathway C.** The third reaction mechanism that has been studied is shown in pathway C of Scheme 1 and can be divided into three steps: (i) deprotonation of the primary intermediate $[L^2Fe^{II}(HOOH)(NCCH_3)]^{2+}$ to form $[L^2Fe^{II}(OOH)(NCCH_3)]^{+}$, (ii) dissociation of acetonitrile to form $[L^2Fe^{II}(OOH)]^{+}$, and (iii) cleavage of the O−O bond in $[L^2Fe^{II}(OOH)]^{+}$ to form an $Fe^{IV}$-oxo-hydroxo complex, $[L^2Fe^{IV}(O)(OH)]^{+}$. As for the previous two pathways, a dissociative mechanism is assumed and steps (ii) and (iii) are considered individually. Not shown in Scheme 1, but also discussed here, is the possibility of ligand exchange of acetonitrile with water to form $[L^2Fe^{II}(OOH)(OH_2)]^{+}$, followed by homolytic cleavage of the O−O bond to form $[L^2Fe^{IV}(O)(OH)]^{+}$ and $H_2O$, analogous to the formation of $[L^2Fe^{IV}(OH)_2]^{2+}$ from $[L^2Fe^{II}(HOOH)(OH_2)]^{2+}$.

Deprotonation of the primary intermediate $[L^2Fe^{II}(HOOH)(NCCH_3)]^{2+}$ leads to the formation of an $Fe^{II}$-hydroperoxo

**Table 4.** Selected Geometric Parameters, O−O Stretching Frequencies, and Relative Energies of the Spin States in the $Fe^{II}$-hydroperoxo Complexes of $L^2$

| | bond distances (Å) | | | | | |
|---|---|---|---|---|---|---|
| | Fe−O1 | Fe−O2 | O1−O2 | $\nu$ ($cm^{-1}$) O1−O2 | $\Delta G^a$ (kJ/mol) 0 K | $\Delta G'^b$ (kJ/mol) 0 K |
| | | | $[L^2Fe^{II}(NCCH_3)(OOH)]^+$ | | | |
| $S=0$ | 1.896 | 2.849 | 1.483 | 860 | 83.0 | 98.1 |
| $S=1$ | 1.815 | 2.853 | 1.478 | 826 | 54.3 | 69.3 |
| $S=2$ | 1.902 | 2.777 | 1.472 | 894 | 0.0 | 15.1 |
| | | | $[L^2Fe^{II}(OOH)]^+$ | | | |
| $S=0$ | 1.903 | 2.021 | 1.482 | 850 | 57.2 | 57.2 |
| $S=1$ | 1.795 | 2.796 | 1.475 | 848 | 14.9 | 14.9 |
| $S=2$ | 1.897 | 2.417 | 1.472 | 871 | 0.0 | 0.0 |
| | | | $[L^2Fe^{II}(OH_2)(OOH)]^+$ | | | |
| $S=0$ | 1.914 | 2.830 | 1.500 | 800 | 91.6 | 92.7 |
| $S=1^c$ | 1.636 | 2.303 | 2.130 | | 53.6 | 54.8 |
| $S=2$ | 1.916 | 2.815 | 1.479 | 855 | 0.0 | 1.1 |

[a] Energy relative to the most stable spin state of complexes with identical ligand sphere. [b] Energy relative to the most stable complex and electronic structure. [c] $[L^2Fe^{II}(OH_2)(OOH)]^+$ in the $S=1$ state converges to a structure best described as a $[L^2Fe^{III}(O)(OH_2)]^+\cdots OH$ species.

intermediate. The geometry of $[L^2Fe^{II}(OOH)(NCCH_3)]^+$ was optimized in all possible spin states, and an $S=2$ ground state is calculated, with relative energies of 54.3 and 83.0 kJ/mol for the $S=1$ and $S=0$ states, respectively. Deprotonation of the bound hydrogen peroxide weakens the O−O bond slightly, which is reflected in the increase in bond length from 1.452 Å in $[L^2Fe^{II}(HOOH)(NCCH_3)]^{2+}$ to 1.472 Å in $[L^2Fe^{II}(OOH)(NCCH_3)]^+$ but has a drastic effect on the Fe−O bond, decreasing the bond length from 2.232 to 1.902 Å. The same tendency is observed in the Fe−O and O−O stretching frequencies. The O−O stretching frequency decreases from 911 to 895 $cm^{-1}$, while the Fe−O stretching frequency more than doubles, from 236 $cm^{-1}$ in the primary intermediate $[L^2Fe^{II}(HOOH)(NCCH_3)]^{2+}$ to 505 $cm^{-1}$ in $[L^2Fe^{II}(OOH)(NCCH_3)]^+$. These results are summarized in Table 4, together with the geometries of $[L^2Fe^{II}(OOH)(OH_2)]^+$ and $[L^2Fe^{II}(OOH)]^+$.

Deprotonation of $[L^2Fe^{II}(HOOH)(NCCH_3)]^{2+}$ by $H_2O$, to form $[L^2Fe^{II}(OOH)(NCCH_3)]^+$ and $H_3O^+$ (eq 5), has a highly unfavorable reaction energy of +128.7 kJ/mol.

$$[L^2Fe^{II}(HOOH)(NCCH_3)]^{2+} + H_2O \rightarrow [L^2Fe^{II}(OOH)(NCCH_3)]^+ + H_3O^+ \quad (5)$$

The dissociation of the $CH_3CN$ molecule coordinated trans to N7 in $[L^2Fe^{II}(OOH)(NCCH_3)]^+$ is exothermic by −15.1 kJ/mol. A quintet ground state is calculated for $[L^2Fe^{II}(OOH)]^+$, and the triplet and singlet states have energies of 14.9 and 57.2 kJ/mol with respect to the ground state. Acetonitrile dissociation to form $[L^2Fe^{II}(OOH)]^+$ causes a further increase of the O−O bond length from 1.472 Å in $[L^2Fe^{II}(OOH)(NCCH_3)]^+$ to 1.484 Å in $[L^2Fe^{II}(OOH)]^+$ and a decrease of the Fe−O bond length from 1.902 to 1.897 Å. Again, this is reflected in the Fe−O and O−O stretching frequencies (see Table 4).

Homolytic cleavage of the O−O bond in $[L^2Fe^{II}(OOH)]^+$ is both thermodynamically and kinetically the most favorable

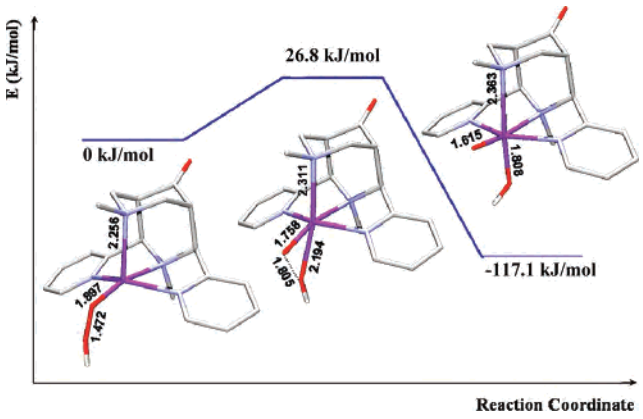


**Figure 7.** The $S=2$ reaction profile for heterolytic cleavage of the O−O bond in $[L^2Fe^{II}(OOH)]^+$.

**Scheme 5**

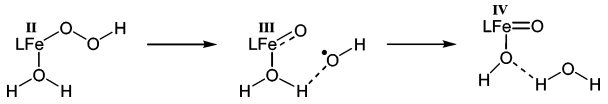


of all direct O−O bond cleavage reactions studied, with a total reaction energy of −117.1 kJ/mol and an energy barrier of 26.8 kJ/mol. As for $[L^2Fe^{IV}{=}O(OH_2)]^{2+}$, the product of this reaction, an $[L^2Fe^{IV}{=}O(OH)]^+$ complex, has an $S=2$ ground state with the $S=1$ spin state lying 24.5 kJ/mol higher in energy. The energies of this reaction and the structures of the reactant, transition state, and product are shown in Figure 7. The geometry of the transition state is quite remarkable, with an Fe−O−O angle of 116.1°, around 25° larger than the corresponding angle in both the reactant and the product (90.5° and 91.6°, respectively).

As for the previous two mechanisms, the fact that the O−O bond cleavage is homolytic in nature is confirmed by the buildup of spin density on the oxygen atom of the formed •OH radical (−0.28) in the transition state. The iron-bound oxygen atom also has significant spin density (0.23), in keeping with the formation of an Fe−O double bond, as was the case for $[L^2Fe^{III}(OOH)]^{2+}$.

An important difference between this and the previous two mechanisms is that all intermediates along this pathway have an $S=2$ ground state, and no forbidden spin-crossovers occur. This, in addition to the exothermic solvent abstraction, the exothermic reaction energy and low-energy barrier for O−O bond cleavage, and the relatively few steps required, makes this pathway extremely attractive. The only real problem is therefore the deprotonation of $[L^2Fe^{II}(HOOH)(NCCH_3)]^{2+}$.

If an additional water molecule is used to stabilize the released proton through hydrogen-bonding however (eq 6), the barrier for the deprotonation of $[L^2Fe^{II}(HOOH)(NCCH_3)]^{2+}$ is lowered by almost 88 kJ/mol to +40.8 kJ/mol.

$$[L^2Fe^{II}(HOOH)(NCCH_3)]^{2+} + H_4O_2 \rightarrow [L^2Fe^{II}(OOH)(NCCH_3)]^+ + H_5O_2^+ \quad (6)$$

If a third water molecule is included to stabilize the released proton, the reaction becomes slightly exothermic

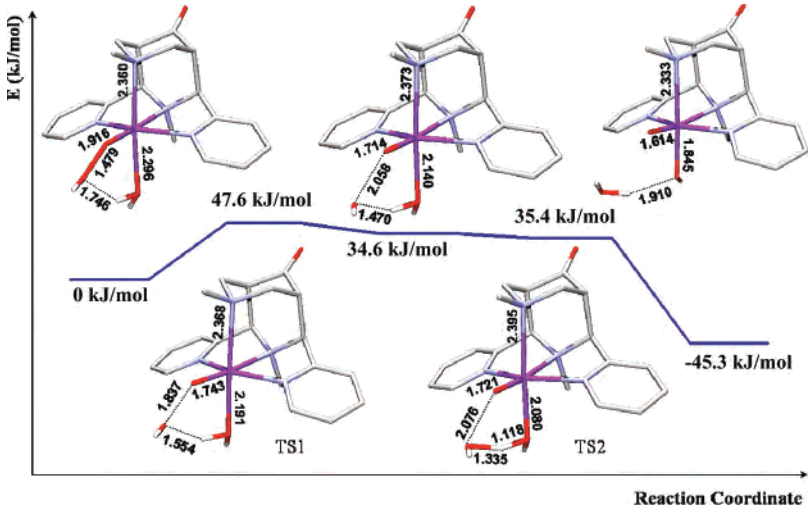


**Figure 8.** The $S = 2$ reaction profile for homolytic cleavage of the O−O bond in $[L^2Fe^{II}(OOH)(OH_2)]^+$.

**Table 5.** Summary of the Bond Distances and Mulliken Spin Densities for the Reaction of $[L^2Fe^{II}(OOH)(OH_2)]^+$ to $[L^2Fe^{IV}(O)(OH)]^+\cdots OH_2$

| | bond distance (Å) | | | Mulliken spin density | | | |
|---|---|---|---|---|---|---|---|
| complex | Fe−O1 | O1−O2 | Fe−O3 | Fe | O1 | O2 | O3 |
| $[LFe^{II}(OOH)(OH_2)]^{2+}$ | 1.916 | 1.479 | 2.269 | 3.77 | 0.11 | 0.01 | 0.02 |
| TS1 | 1.743 | 1.837 | 2.191 | 3.93 | 0.26 | −0.42 | 0.04 |
| $[LFe^{III}(O)(OH_2)]^{2+}$ | 1.714 | 2.058 | 2.140 | 4.03 | 0.26 | −0.57 | 0.06 |
| TS2 | 1.721 | 2.076 | 2.080 | 4.06 | 0.15 | −0.52 | 0.07 |
| $[LFe^{IV}(O)(OH)]^{2+}$ | 1.614 | 3.001 | 1.845 | 3.20 | 0.50 | 0.01 | 0.14 |

(+6.6 kJ/mol), and further hydrogen bonding is likely to further decrease the energy. While these hydrogen-bonding energies are only approximate, they show that this reaction is feasible in the presence of water. The p$K_a$ values of the bispidine $Fe^{II}$-hydrogen peroxide complexes are not known, but a p$K_a$ of 7.6 has been experimentally determined for $[L^3Fe^{II}(OH_2)]^{2+}$.[15] From this value and the known p$K_a$ values of $H_2O$ (15.7) and $H_2O_2$ (11.7), the p$K_a$ value of $[L^3Fe^{II}(HOOH)]^{2+}$ is estimated to be in the region of 4. One expects the p$K_a$ of $[L^2Fe^{II}(HOOH)(NCCH_3)]^{2+}$ to lie in the same range, which implies an easy deprotonation of the species even at pH values below 7. This agrees with the exothermic reaction energy predicted in the presence of three or more water molecules and indicates that this is probably the favored reaction pathway in aqueous solution. As the $H_2O_2$ solution contains water (30% aqueous solution), there will be enough water available for the deprotonation step.

Analogous to the formation of $[L^2Fe^{IV}(OH)_2]^{2+}$ from $[L^2Fe^{II}(HOOH)(OH_2)]^{2+}$, the $[L^2Fe^{IV}{=}O(OH)]^+$ complex can also be formed from $[L^2Fe^{II}(OOH)(OH_2)]^+$, as shown schematically in Scheme 5.

As discussed previously, the dissociation of $CH_3CN$ is exothermic by −18.7 kJ/mol and coordination of a $H_2O$ molecule trans to N7 is approximately thermoneutral (1.1 kJ/mol). The formed $[L^2Fe^{II}(OOH)(OH_2)]^+$ complex also has an $S = 2$ ground state with relative energies of 53.7 and 91.6 kJ/mol for the $S = 1$ and $S = 0$ spin states, respectively. The reaction pathway for the reaction of $[L^2Fe^{II}(OOH)(OH_2)]^+$ to $[L^2Fe^{IV}{=}O(OH)]^+\cdots OH_2$ on the quintet surface is shown in Figure 8, and relevant bond lengths and Mulliken spin densities are given in Table 5.

The first step, O−O bond cleavage in $[L^2Fe^{II}(OH_2)(OOH)]^+$, has a relatively high-energy barrier of 47.6 kJ/mol and is endothermic by 38.2 kJ/mol, compared to an energy barrier of 26.8 kJ/mol and a total reaction energy of −117.1 kJ/mol for the O−O bond cleavage in $[L^2Fe^{II}(OOH)]^+$. The $Fe^{III}$ oxidation state of the $[L^2Fe^{III}{=}O(OH_2)]^+\cdots OH$ intermediate is confirmed by the Mulliken spin density on the iron center, which increases from 3.77 in $[L^2Fe^{II}(OH_2)(OOH)]^+$ to 4.03 in $[L^2Fe^{III}{=}O(OH_2)]^+\cdots OH$, closer to the spin densities of 4.21 and 4.19 found on the iron center in $[L^2Fe^{III}(OH)(NCCH_3)]^{2+}$ and $[L^2Fe^{III}(OOH)(NCCH_3)]^{2+}$ than to that of the $Fe^{II}$ reactant. The formation of the $^{\bullet}OH$ radical can also be seen from the change in spin density on O2.[43,44]

It is interesting to compare the spin densities on Fe and O2 in this transition state (TS1 in Table 5 and Figure 8) with the corresponding transition state in the reaction of $[L^2Fe^{II}(OH_2)(HOOH)]^{2+}$ to $[L^2Fe^{III}(OH)(OH_2)]^+\cdots OH$ (see Figure 8). In the transition state for O−O bond cleavage in $[L^2Fe^{II}(OH_2)(HOOH)]^{2+}$, the spin density on Fe is decreased relative to the reactant and an α-electron is removed from the O−O bond to form an $^{\bullet}OH$ radical (the spin density on O2 is positive), which is indicative of a spin-crossover from an $S = 2$ to an $S = 1$ state. In contrast, the transition state for O−O bond cleavage in $[L^2Fe^{II}(OOH)(OH_2)]^+$ shows an increase in spin density on Fe relative to the reactant, and a $\beta$-electron is removed from the O−O bond to form the $^{\bullet}OH$ radical (the spin density on O2 is negative), indicating that no spin-crossover takes place.

The $[L^2Fe^{III}{=}O(OH_2)]^+\cdots OH$ intermediate is unstable and reacts further to form $[L^2Fe^{IV}{=}O(OH)]^+\cdots OH_2$, a reaction which releases 83.5 kJ/mol. However, the transition state for this reaction (TS2) is calculated to have an energy of 35.4 kJ/mol relative to the reactant, which is lower than the energy

(43) While the assignment of double-bond character to Fe=O is somewhat arbitrary, the bond length of 1.714 Å is much closer to the bond length of 1.614 Å in the $Fe^{IV}{=}O$ product than to that of 1.916 Å in the $Fe^{II}$ reactant. More significantly, it is slightly shorter than the Fe−O bond length in $[L^2Fe^{III}(OH)(NCCH_3)]^{2+}$ and 0.1 Å shorter than the terminal Fe−O distance in the only characterized $Fe^{III}{=}O$ complex.

(44) MacBeth, C. E.; Golombek, A. P.; Young V. G., Jr.; Kuczera, K.; Hendrich, M. P.; Borovik, A. S. *Science* **2000**, *289*, 938.

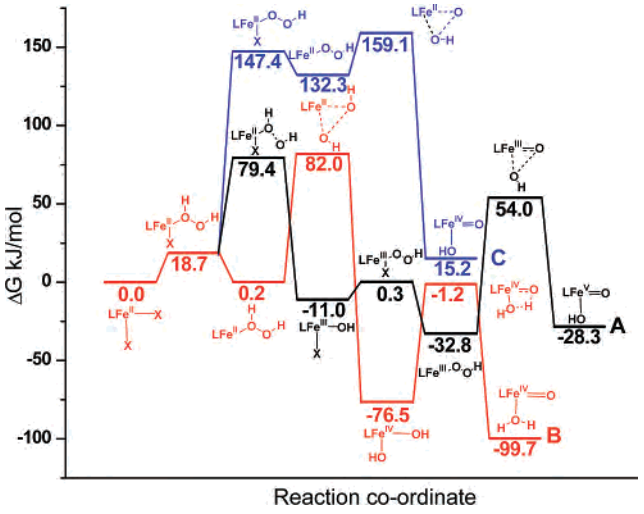


**Figure 9.** Summary of the three main reaction mechanisms studied.

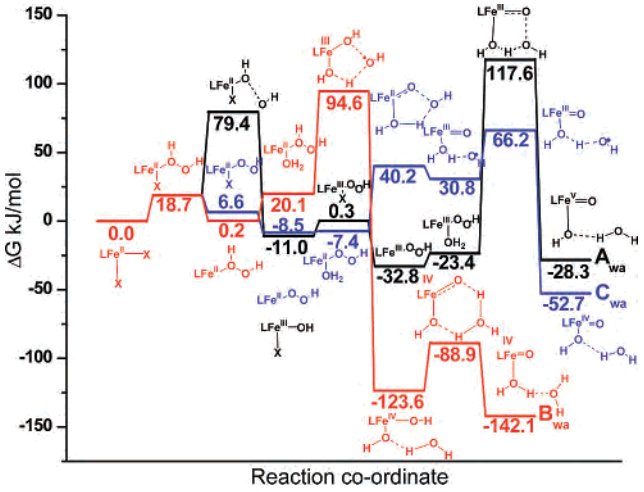


**Figure 10.** Summary of the three main water-assisted reaction mechanisms.

of the $[L^2Fe^{III}{=}O(OH_2)]^{+}\cdots OH$ intermediate. A comparison of the geometries reveals that TS2 is out of place in the general trend in the bond lengths along the reaction coordinate. For example, the Fe−O1 bond lengths decrease steadily from $[L^2Fe^{II}(OH_2)(OOH)]^{+}$ to $[L^2Fe^{IV}{=}O(OH)]^{+}\cdots OH_2$, with the exception of TS2, in which the Fe−O bond is slightly longer than in the $Fe^{III}$ intermediate. This is an indication of the shallowness of the PES in this region rather than a significant error.

The total energy of this reaction is −45.3 kJ/mol, which is much smaller than the reaction energy of the direct O−O bond cleavage in $[L^2Fe^{II}(OOH)]^{+}$ (−117.1 kJ/mol). This is partially due to the energy released upon formation of $[L^2Fe^{II}(OH_2)(OOH)]^{+}$ from $[L^2Fe^{II}(OOH)]^{+}$ and $H_2O$ but also due to the fact that the $[L^2Fe^{IV}{=}O(OH)]^{+}\cdots OH_2$ product is 72.9 kJ/mol higher in energy than $[L^2Fe^{IV}{=}O(OH)]^{+}$ and $H_2O$. A comparison of the geometries of $[L^2Fe^{IV}{=}O(OH)]^{+}$ and $[L^2Fe^{IV}(O)(OH)]^{+}\cdots OH_2$ reveals that the Fe−O3 bond length (O3 is the oxygen atom from the trans to N7 bound $H_2O$) is significantly longer in the hydrogen-bonded complex and the O3 bound proton is rotated by ∼180° from the ground state geometry of $[L^2Fe^{IV}{=}O(OH)]^{+}$.

## Conclusion

Three possible mechanisms (pathways A−C in Scheme 1) have been investigated for the reaction of the $Fe^{II}$ complex of the tetradentate bispidine ligand $L^2$ with $H_2O_2$, and these are summarized in Figure 9. The water assisted pathways for the three mechanisms are shown in Figure 10.

Pathway A is unlikely to take place in the $Fe^{II}/L^2/H_2O_2$ system due to the high barrier calculated for the conversion of $[L^2Fe^{II}(HOOH)(NCCH_3)]^{2+}$ to $[L^2Fe^{II}(OH)(NCCH_3)]^{2+}$ (79.4 kJ/mol, water-free and water-assisted) and the conversion of $[L^2Fe^{III}(OOH)]^{2+}$ to $[L^2Fe^{V}{=}O(OH)]^{2+}$ (86.8 kJ/mol, water-free; 150.4 kJ/mol, water-assisted) and higher overall reaction energies compared to the favorable $Fe^{II}/Fe^{IV}$ alternatives found for pathways B and C.

In the water-assisted and water-free versions, pathway B is the thermodynamically most favorable mechanism. The first step is proposed to be the formation of the primary intermediate $[L^2Fe^{II}(HOOH)(NCCH_3)]^{2+}$. Due to the dissociative nature of $Fe^{II}$ ligand exchange reactions and the weak binding of the trans to N7 coordinated solvent molecule, a pentacoordinate $[L^2Fe^{II}(HOOH)]^{2+}$ intermediate is formed. This undergoes homolytic cleavage of the O−O bond to form $[L^2Fe^{IV}(OH)_2]^{2+}$. Proton transfer from the hydroxide bound trans to N3 to that trans to N7 in $[L^2Fe^{IV}(OH)_2]^{2+}$ leads to the formation of the high-valent $[L^2Fe^{IV}{=}O(OH_2)]^{2+}$ product, which may also undergo ligand exchange to form $[L^2Fe^{IV}{=}O(NCCH_3)]^{2+}$. In the water-assisted path, the pentacoordinate $[L^2Fe^{II}(HOOH)]^{2+}$ intermediate adds a water molecule, and then the cleavage of the O−O bond takes place. The coordination of water is endothermic, but the formation of $[L^2Fe^{IV}(OH)_2]^{2+}\cdot\cdot OH_2$ is significantly more exothermic compared to the non-water-assisted path. The formation of $[L^2Fe^{IV}{=}O(OH_2)]^{2+}$ from $[L^2Fe^{IV}(OH)_2]^{2+}\cdot\cdot OH_2$ is also a facile reaction in the water-assisted mechanism.

Without water, for path C the deprotonation of the $[L^2Fe^{II}(HOOH)(NCCH_3)]^{2+}$ species is very endothermic and unlikely to take place. However, in the water-assisted pathway the reaction energies are reduced to thermoneutral conditions. The energetics of the following steps are not prohibitively high, and therefore, in the presence of water, the formation of $[L^2Fe^{IV}{=}O(OH)]^{+}$ is also likely.

The facile direct formation of $[L^2Fe^{IV}(OH)_2]^{2+}$ may explain why in the $Fe^{II}/L^2/H_2O_2$ system no $Fe^{III}$ intermediates and ferryl products have been observed so far. It is tempting to suggest that $[L^2Fe^{IV}(OH)_2]^{2+}$ is the favored oxidant for diol formation in the oxidation of olefins, and this would explain some of the striking differences in reactivity and product distribution between the $L^2$- and $L^4$-based systems (see Introduction).[18] It is important to note that the $[LFe^{IV}(OH)_2]^{2+}$ intermediate, essential to our mechanistic proposal, cannot be formed when L is a pentadentate ligand. The analogous reaction for a pentadentate ligand (e.g., $L^3$ or $L^4$) leads to the formation of $[LFe^{III}(OH)]^{2+}$ and $^{\bullet}OH$, the first step in the formation of the $[LFe^{III}(OOH)]^{2+}$ intermediates observed for $L^3$ and $L^4$. Therefore, the open coordination site is the crucial element in the differences in product distribution observed between the $L^2$- and $L^4$-based catalyst systems.

However, $Fe^{III}$-hydroxo and $Fe^{III}$-hydroperoxo intermediates have also been observed for tetradentate ligands such as tpa. The deciding difference between $L^2$ and other tetradentate systems may be the weak trans to N7 ligand binding in the $L^2$ complex, enforced by the demands of the rigid ligand backbone,[45] which induces the reactive five-coordinate intermediate.

(45) Atanasov, M.; Comba, P. To be submitted for publication.

**Acknowledgment.** Financial support by the German Science Foundation (DFG) and an AvH fellowship to G.R. are gratefully acknowledged.

**Supporting Information Available:** The geometries of the computed structures of the reactant, transition state, and products. This material is available free of charge via the Internet at http://pubs.acs.org.

IC061129Y